esteem3

Enabling Science through European Electron Microscopy

First report on TEM methods applied to materials for energy

Deliverable D8.1 – version 8

Estimated delivery date: M16 April 2020

Actual delivery date: M16 April 2020

Lead beneficiary: CAD, JSI

Person responsible: Susana Trasobares and Miran Ceh

Deliverable type: ☒ R ☐ DEM ☐ DEC ☐ OTHER ☐ ETHICS ☐ ORDP

Dissemination level: ☒ PU ☐ CO ☐ EU-RES ☐ EU-CON ☐ EU-SEC

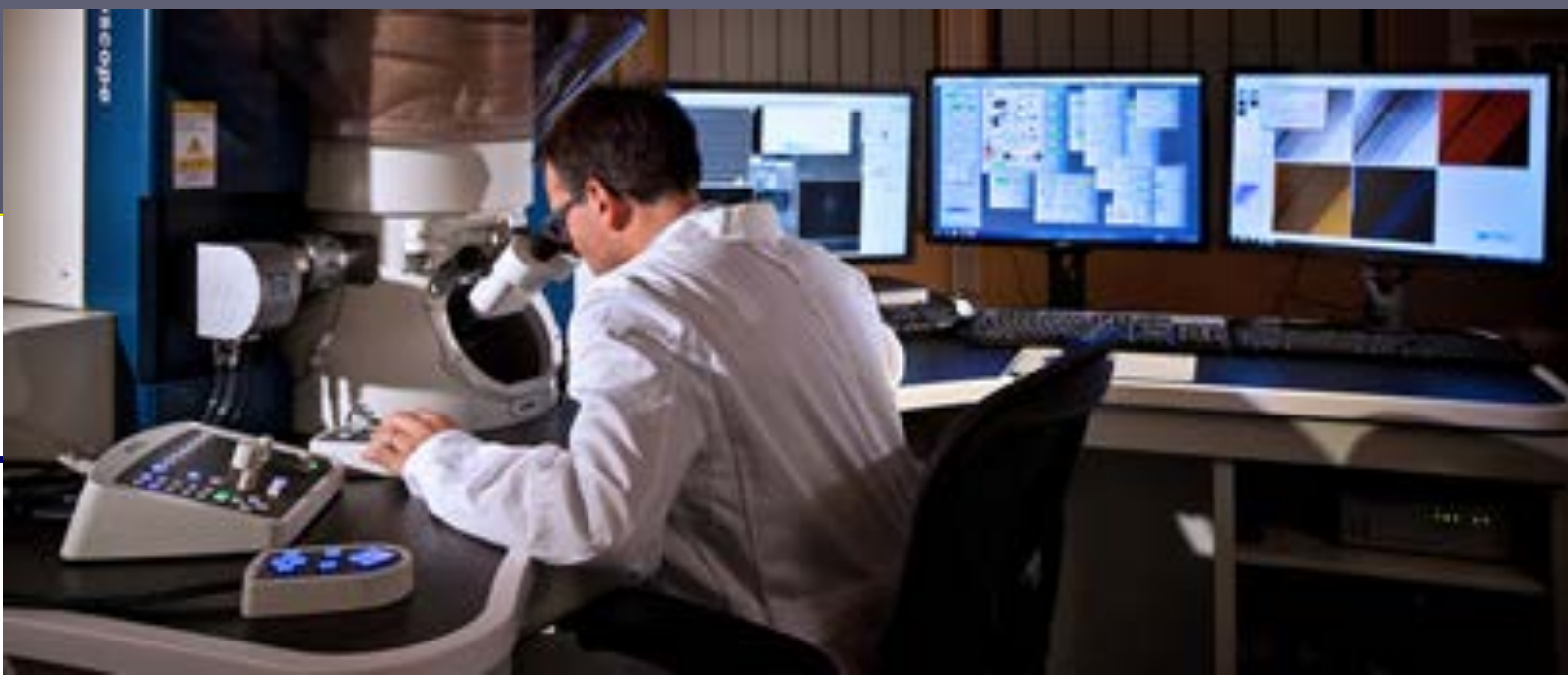

THIS PROJECT HAS RECEIVED FUNDING FROM THE EUROPEAN UNION'S HORIZON 2020 RESEARCH AND INNOVATION PROGRAMME UNDER GRANT AGREEMENT NO **823717**

Grant Agreement No:	823717
Funding Instrument:	Research and Innovation Actions (RIA)
Funded under:	H2020-INFRAIA-2018-1: Integrating Activities for Advanced Communities
Starting date:	01.01.2019
Duration:	48 months

Table of contents

Revision history log

Version number	Date of release	Author	Summary of changes
V0.1	02/03/2020	S Trasobares	Template
V0.2	19/03/2020	Adam Kruczek	Task 8.3
V0.3	27/03/2020	S Trasobares	Task 8.1 and 8.2
V0.4	01/04/2020	G Nicotra	Task 8.3 and 8.4
V0.5	02/04/2020	S Boninelli	Task 8.1, 8.2, 8.3
V 0.6	03/04/2020	S Trasobares	Unified format
V 0.7	06/04/2020	M Ceh	Tasks 8.1, 8.2, 8.4, unified format
V 0.8	06/04/2020	S Trasobares	unified format and references
V 0.9	15/04/2029	L Guilloteau	Editing
V 1.1	16/04/2020	P. van Aken	Approval

Context of the present report

Quoted from the proposal:

"Spectroscopy and imaging techniques for quantitative structural and chemical characterization of materials will be applied to a range of energy materials. This WP will use in-situ capabilities to perform dynamic characterisation of materials for energy and will develop sample preparation recipes specific to these systems, including the key issue of anaerobic sample environments for new battery materials".

Deliverable D8.1 belongs to WP8 Materials for Energy. In this work package, four different tasks have been included. Here in we will describe the progress carried out in every task.

Task 8.1 Nanomaterials for Sustainable Development

1.- ZnO nanostructures.

HAADF Imaging and state-of-the-art spectroscopy techniques as EDX, EELS, and CL, have been combined to understand the photocatalytic behaviour of ZnO:Ce nanostructures (Figure 1). In particular, the addition of Ce ions into the ZnO nanostructure did not change the structural morphology of the system, however the synthesised material has promising photocatalytic properties, having a better photocatalytic performance that the obtained on a reference sample as TiO_2-P25.
As indicated at the ESTEEM3 proposal, in the case of photocatalytic materials there is a lack of nano-optical characterisation. In this context, UCA and ORS partners have worked together in order to performed CL measurements on ZnO:Ce nanostructures, nevertheless luminescence signal was not detected, it could be due to the possible presence of defects at the nanostructure, It is known that point defects as for example oxygen vacancies [1] strongly reduce the luminescence signal.

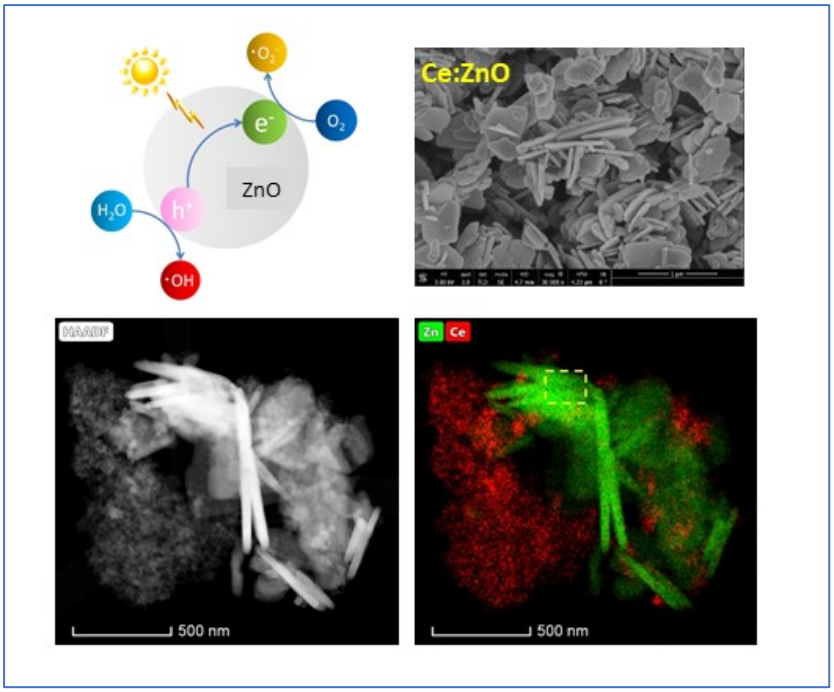

Figure 1. HAADF imaging (SEM ad STEM) and STEM-EDX spectroscopy on Ce :ZnO nanostructires. (Ce signal in red and Zn signal in green)

In the last few years, ZnO nanorods (NRs) have been studied for many types of applications, such as energy harvesting, UV detection, and biosensing. Chemical Bath Deposition (CBD) is a fast and low-cost technique which allows to efficiently grow a large amount of NRs [(~3.7±0.5) x10^9 NRs/cm^2], whose mean length and diameter are equal to (755±55) nm and to (67± 20) nm, respectively.
Scanning Electron Microscopy allowed us to distinguish the occurrence of two families of ZnO NRs: (i) NRs grown on the seeded substrate and (ii) NRs grown in solution by spontaneous homogeneous nucleation. Representative SEM plan views of the as grown sample is shown in Figure. 2, where an aggregate of micrometers large ZnO NRs grown by spontaneous and homogeneous nucleation in solution lye on a NR forest growing from the substrate.

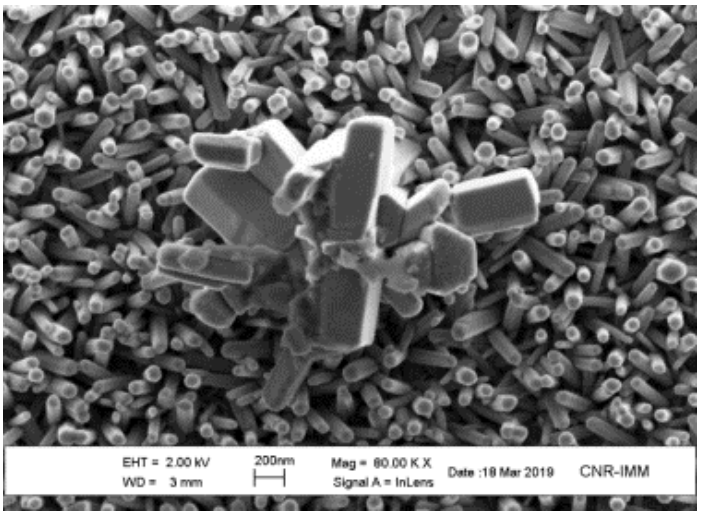

Figure 2.- SEM of the sample showing an aggregate of large ZnO NRs grown in solution and lying on a "forest" of NRs.

Recent studies demonstrated the existence of surface radiative deep level defects in CBD grown ZnO NRs, whose light emission can be engineered by proper annealing processes. The aim of our work is to study the tuning of light emission as a function of different thermal annealing processes (O_2 and Ar ambient) and to map of the corresponding light emitting centres.

A comprehensive structural, chemical and optical characterization based on the combination of TEM and SEM-based techniques demonstrate that cathodoluminescence (CL) spectrum (Figure 3a) shows a sharp peak in the UV and a broad band in visible range. These signals are associated, respectively, to carriers recombination in correspondence to near band gap (associated to the ZnO NR core) and deep level defect states (associated to superficial defects states), as demonstrated by the CL maps reported in Figure 3b

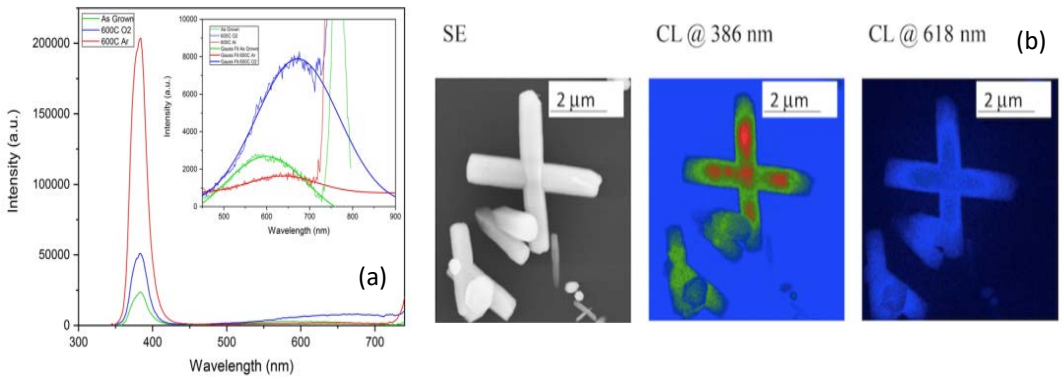

Figure 3.- (a) Cathodoluminescence spectra of as-grown ZnO NRs show two main features: a sharp peak in the UV region and a broad band in the visible region. After the annealing, the UV peak position is unchanged while a red shift is noted in the

visible range after annealing. (b) Secondary electron (SE) and CL maps acquired respectively, at 386 nm and 618 nm demonstrate that the UV emission comes mainly from the ZnO NR core, while the visible light originates from the surface.

One of possible methods to synthesise ZnO nanostructures with high surface is based on relatively old method of anodic oxidation of metal Zn, although this method is preferentially applied to anodization of Al and Ti. Our recent experiments showed that anodic oxidation of metal Zn surfaces (foils, mesh, wires) yields various shapes of ZnO nanostructures grown on the Zn surface. Depending on changing main anodization parameters (applied voltage, time, electrolyte composition, etc.) it was possible to obtain either nanorods or flower like morphologies (Figure 4).

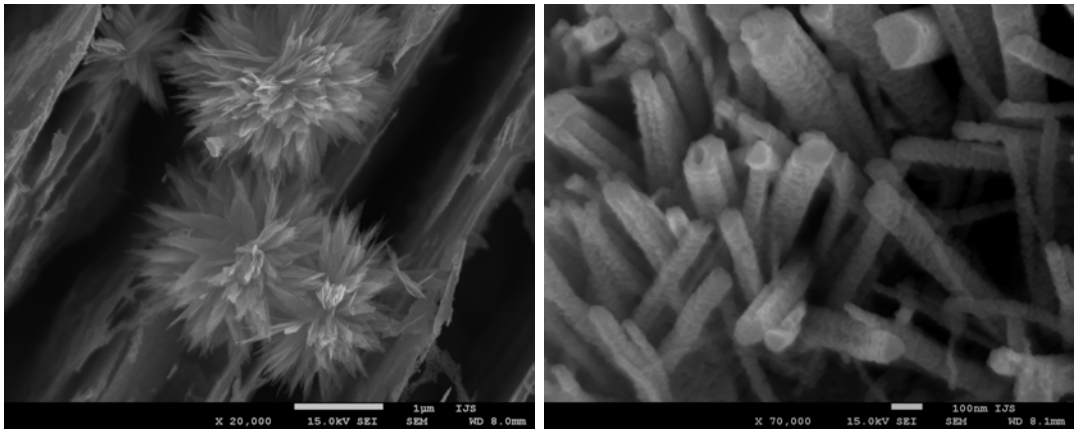

Figure 4. (a) ZnO grown in the shape of flowers. The sample is fully crystalized (b) Changing of the electrolyte causes growth of ZnO nanorods that have nucleated and grown from the starting nucleated crystal. The nanorods are polycrystalline in nature with the estimated grain size in the nanometer range.

2.- TiO_2 nanostructures

It is well known that photocatalysis is a very promising, so-called advanced oxidation process (AOP) that can be readily used for photocatalytic decomposition of organic compounds into their basic constituents, such as carbon dioxide, water and inorganic ions. However, our recent investigations have shown that the process of photoelectrocatalysis is even more efficient in decomposition of organic compounds due to slower recombination of light-generated electron/holes pairs as compared to the process of photocatalysis. Additional potential between the photoanode (photocatalyst) and cathode material assures longer contact times of reactive radicals with organic compounds thus increasing decomposition efficiency. The most widely used and extensively studied photocatalyst is titanium dioxide (TiO_2), which is highly photoactive when illuminated with UV light (λ<390 nm). TiO_2 in photocatalytic reactors is usually used in the form of suspended (nano)particles or in the form of more or less porous TiO_2 films on a carrier support. However, only extremely firm contact of TiO_2 film with electrically conductive substrate enables such structure to be used as photoanode in photoelectrocatalysis, where external electric voltage is applied between photoanode and cathode material. To our understanding anodic oxidation of metal titanium is one of rare methods that enables structural ingrowth of TiO_2 nanotubes with metallic conductive substrate (Figure 5).

In our recent work phenol photocatalysis, electrocatalysis and photoelectrocatalysis were performed under different conditions (UV-light intensity, applied electrical potential, and flow rate) inside an in-house-developed, coiltype, photoelectrocatalytic microreactor. The main part of the microreactor is a photocatalytically active unit that was placed into a channel in a UV-transparent housing. The degradation reactions took place on the surface of a photoanode coil that is made up of TiO2 nanotubes. The mechanisms of photocatalysis and photoelectrocatalysis were proposed and validated with a mathematical model, which described the governing processes occurring during the microreactor's

operation. In the case of the photocatalysis there was not enough oxygen for complete phenol degradation, whereas phenol was successfully mineralized with the help of an applied electrical potential. The applied electrical potential successfully prevented electron–hole recombination, which allowed for unhindered hydroxyl radical formation and a high phenol degradation rate. The highest initial phenol concentration used, approximately 45.7 mg/l, was completely mineralized at an applied potential of 16 V, a UV-light intensity of approximately 2.8mW/cm^2, and a flow rate of 50 µL/min. Finally, an energy-efficiency study was performed to identify the optimal photoelectrocatalytic microreactor's operating conditions for the phenol degradation. The composition of the electrolyte on the overall photocatalytic properties of anodized TiO2 nanotubes was also evaluated [2]

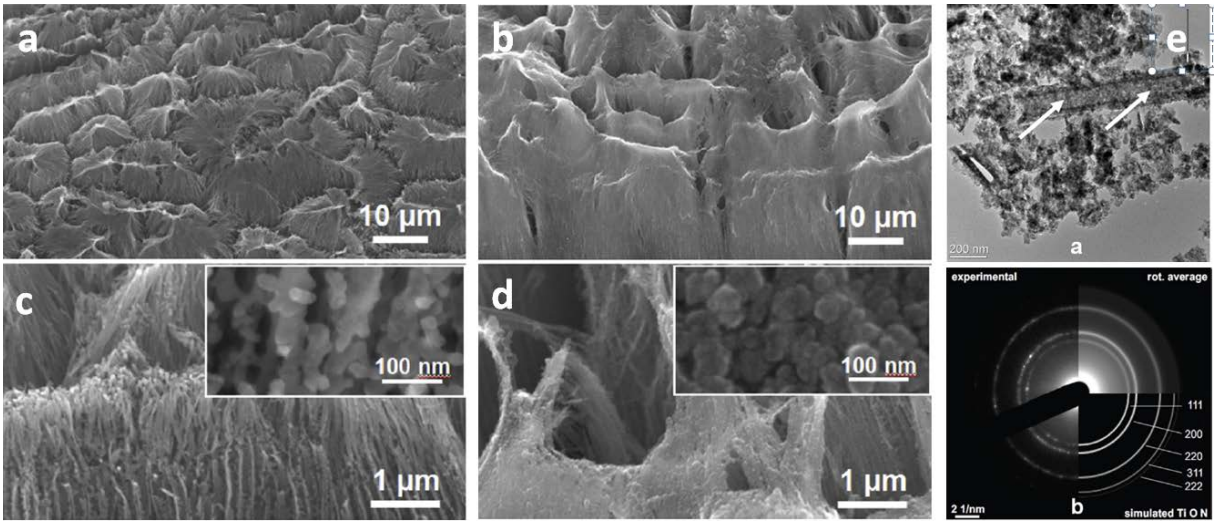

Figure 5.- (a-d) Various TiO2 nanotubes surface morphologies prior and after photoelectrocatalytic degradation of phenol. (e) TEM BF micrograph of a TiO2 nanotube with the corresponding SAED pattern confirming the anatase structure of TiO2 nanotubes.

3.- Oxygen evolution on beam sensitive energy hollandite nanomaterials.

Understanding the structural and chemical nature of materials for energy with reduced dimensionality requires pushing the limits of characterization methodologies and the development of new strategies. Specifically, the quantification of light elements is a challenge task. Electron tomography and EDX spectroscopy have been combined to estimate z-factors from theoretical cross-section for Super-X G2 EDS detector installed on the FEI TITAN Cubed Themis 60-300 microscope at Cadiz University (Figure 6). The estimated Z-factors have been further applied to study the oxygen evolution on beam sensitive hollandite nanomaterials, obtaining an accurate Mn/O quantification $K_{0.13}MnO_{1.95}$ with values similar to those previously obtained by neutron diffraction (Figure 3). This experiment has demonstrated the good synergy stablished between WP5 Task 5.3: Increasing accuracy and reproducibility through correlation and coincidence experiments and WP8 Task 8.2.

Additionally, in the particular case, of applying state of the art electron microscopy to the characterization of several materials with catalytic applications. It has been observed that the addition of a submonolayer coverage of CeO_2 into Au/YSZ catalyst, enhances not only the catalytic activity of the initial system for CO oxidation reaction but also improve its stability against deactivation under prolonged, very high temperature, working conditions. [3]

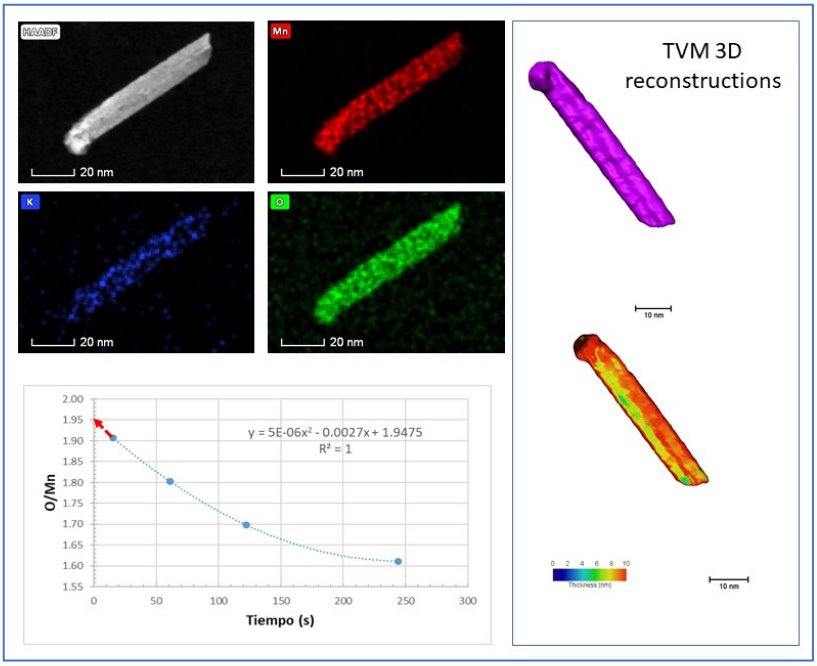

Figure 6.- (a) Representative HAADF-STEM image and EDS elemental mapping showing the distribution of Mn (red), K (blue) and O (green). (b) Electron tomography result obtained from TVM 3D algorithm. 3D volume rendered of the hollandite nanorod together the 3D thickness map are displayed. (c) O/Mn ratio evolution calculated from Z-factors. Extrapolation to time equal to 0

Task 8.2 Dynamic Characterization of Energy Materials

Dynamic characterization of energy materials are performed using in-situ capabilities available in WP6. In addition, new equipment dedicated to energy materials time resolved cathodoluminicense characterization is being developed

1.- Development of a time-resolved CL@SEM

CAT and CNRS-TOU are working on the ***Development of a low energy and time resolved electron microscopy*** project. The goal is to upgrade a Scanning Electron Microscope (SEM), placed in CAT labs, into a Time Resolved (TR) instrument to perform lifetime measurements. The latter can be performed by combining an electrostatic Beam Blanker (BB) and a Cathodoluminescence (CL) system, both already installed in the SEM, Figure 7.

Figure 7.- Scanning Electron Microscope equipped with the CL apparatus in CAT labs

However, being the BB conceived for electron beam lithography, it is driven by its own Raith unit and software, which limits the instrument time response due to gate delay. In order to test the attainable time resolution, we planned to perform some tests by using a SR430 Multichannel Analyser to build up a time-delay histogram. Zinc Oxide (ZnO) nanorods are a suitable specimen thanks to a carrier lifetime (~10^{-1} nsec) lying below the expected instrument time resolution. At the same time, a collaboration with ZEISS is starting to find a more flexible solution to implement TR-CL in SEM and push further the limits of the system. Unfortunately, a series of technical problems (turbomolecular pump failure and UPS breakdown) occurred in the last months, preventing experimental project progresses. Moreover, recently, the access to the laboratories has been strongly restricted because of the global coronavirus emergency. In this context, the activity has been moved towards electron optics simulations through SIMION in order to design a novel BB.

2.- In-situ heating experiment of In^{+3}-doped ZnO

It is known that doping ZnO with 5 valent or 3 valent ions causes the formation of inversion domain boundaries (IDB) in the ZnO structure. These planar defects readily cause exaggerated grain growth of the grains containing such IDB. The structure of these boundaries have been extensively studied, however the initial nucleation stage is still not well explained. In our studies we performed *in-situ* heating experiments where TEM specimen ZnO single crystal was covered with the dopant powder In_2O_3 and heated up to 900ºC in heating holder. The nucleation and growth of the IDB was readily observed and recorded (Figure 8).

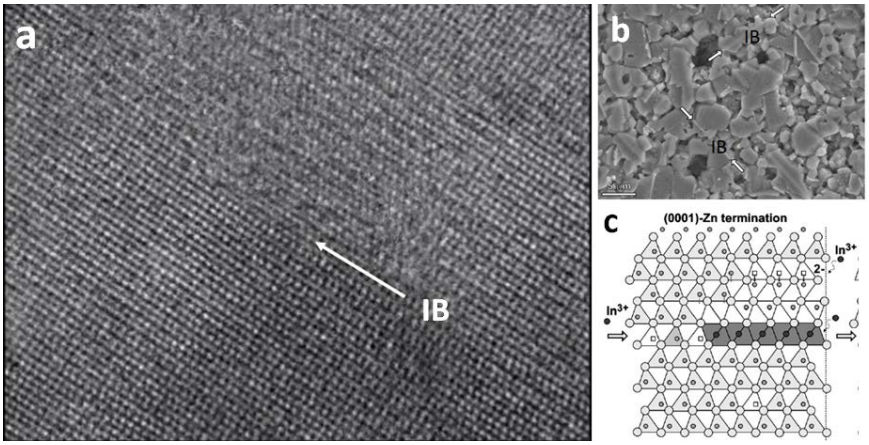

Figure 8.- (a) In-situ excerpt from movie showing a sequence of formation of the IB in In+3 doped ZnO. (b) IB's in In+3 doped polycrystalline ZnO. (c) The structure of the IB.

3.- In-situ LC TEM experiment

Liquid electrochemical holders enable *in-situ* observation of electrochemical reactions in (S)TEM in static or in flow conditions using adjustable potential changes between work electrode and cathode in a three electrode system. The deposition of metal Ni was studied from Ni^{+2} solutions based on recorded oxidation/reduction cyclic voltammograms for electrochemical reaction of Ni/Ni^{+2}. Preliminary experiments showed the nucleation and growth of NI nanoparticles at the Pt working electrode at the potential of -0,9 mV for 100 s (Figure 9).

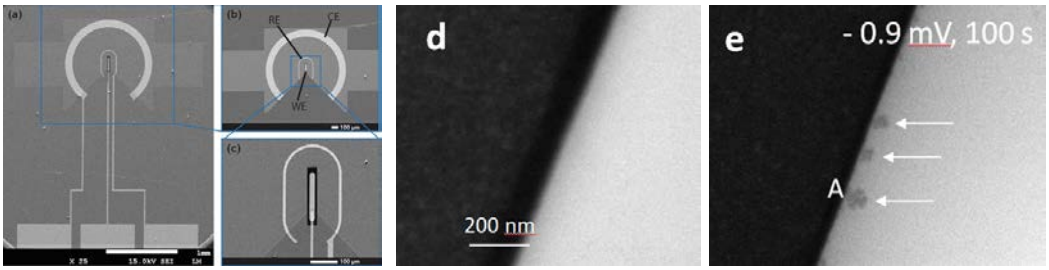

Figure 9.- (a-c) SEM micrograph of three electrode chip system for LC TEM (d) Work electrode before, and (e) after applying potential of -0.9 mV for 100 s. The nucleation of NI nanoparticles can be observed.

Task 8.3: Characterization of Devices for Energy Applications

The following classes of devices for energy applications will be investigated within this task: Thermoelectric generators, Power, RF and energy storage applications, Materials for advanced energy systems

1.-Thermoelectric generators

Thermoelectric generators need a high figure of merit (ZT) in order to perform with high thermal to electric conversion efficiency. Since ZT is determined by the electrical and thermal conductivity and the Seebeck coefficient, and as these properties are inherently interrelated, it is important to understand the correlation between these physical properties and the underlying structure of these devices. In this context, state of the art electron microscopy techniques have been applied for quantitative structural and chemical characterisation of faulted and layered thermoelectric devices. These studies will implement the quantitative methods developed in WP4, where especially the characterisation of phonons will be of high interest.

Three-dimensional characterization of oxide scale on ATI 718Plus® superalloy

ATI 718Plus® (718Plus) is a polycrystalline nickel-based superalloy designed to replace in some application the widely used Waspaloy and Inconel 718 superalloys. It combines excellent mechanical properties with oxidation resistance and workability, which makes it suitable for application in critical rotating components in gas turbines used in aircraft and energy industry. Heat and oxidation resistance of nickel-based superalloys results from the formation of a protective oxide scale, usually Cr_2O_3 or Al_2O_3. However, the extensive chemical composition of nickel-based superalloys (about 10 alloying elements added) leads to the formation of much more complex, multi-layered systems, where chromia and alumina are accompanied by other products of oxidation.

In this study, the evolution of the oxide scale formed on 718Plus superalloy after oxidation at 850 °C up to 4000 hours was investigated. For detailed phases' analysis, analytical electron microscopy was combined with FIB-SEM tomography to not only identify but also show a 3D distribution of phases formed in the near-surface area.

The main factor that caused a change in the chemical and phase composition of 718Plus near its surface was external and internal oxidation. The growth of the protective Cr_2O_3 scale (external oxidation) was associated with a considerable depletion of chromium. As a result, the concentration of chromium directly underneath the scale dropped and led to decomposition of strengthening γ'-

Ni_3(Al, Ti) phase in this area. Simultaneously, internal oxidation of aluminium was observed in this area, leading to the formation of alumina in the chromium depletion zone. Source of aluminium included the η-Ni_6AlNb phase and, to a certain extent, the afore-mentioned γ' phase. Moreover, precipitation of δ-Ni_3Nb phase was observed, which formed an almost continuous layer beneath the chromia scale. Phase distribution and the aforementioned changes in the near-surface area of 718Plus were documented by FIB-SEM tomography (Figure 10). Figure 10a shows the spatial distribution of phases in the near-surface area of 718Plus oxidized at 850 °C for 120 hours, while Figure 10b shows their distribution after 1000 hours.

Detailed microscopical analyses of the through-scale sample revealed a dual-layered structure of the Cr_2O_3 scale in samples oxidized for 120 hours. The outer layer consisted of larger, columnar grains, while the inner one was composed of fine, nanometre-sized equiaxial grains (Figure 10a, c). It is worth mentioning, that after 1000 hours of oxidation chromia scale was composed only of equiaxial grains. Figure 11b shows selected area electron diffraction pattern from the area marked as 1 in Figure 11a, showing a solution for Cr_2O_3 in a $[21\bar{3}0]$ zone axis. Figure 11d shows the high-resolution STEM-HAADF image of a Cr_2O_3 nanostructure at the atomic level, as seen along the $[2\bar{1}\bar{1}0]$ plane, with a simulated arrangement of Cr_2O_3 atomic columns, is superimposed. Detailed analysis of sample oxidized for 120 hours may be found in the article published in *Scripta Materialia [4]*

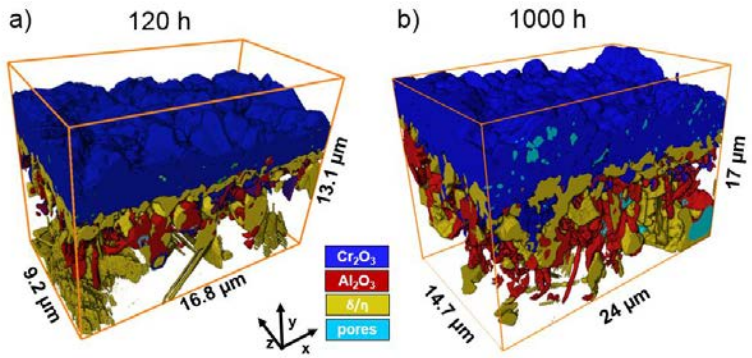

Figure 10.- 3D visualization of the microstructure of the oxide scale formed on the 718Plus superalloy after oxidation at 850 °C, rendered via tomographic reconstruction; a) after 120 hours of oxidation; b) after 1000 hours of oxidation

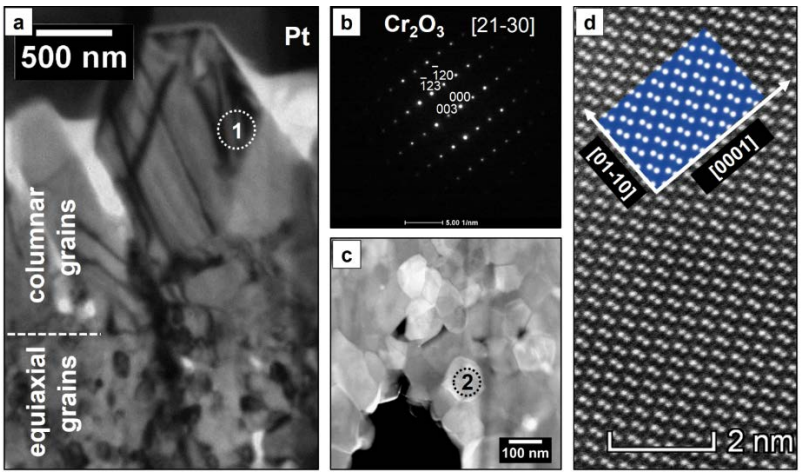

Figure 11. Micro- and nanostructure of the oxide scale formed on 718Plus superalloy after oxidation at 850 °C for 120 h; a) TEM-BF image showing dual-layered scale microstructure; b) Selected area electron diffraction pattern taken from the area marked in Fig. 11a c) STEM-HAADF image showing equiaxial nanometric Cr_2O_3 grains ; d) High-resolution STEM-HAADF image

showing the arrangement of chromium atom columns in the grain marked in Fig. 11c, with a corresponding simulated HAADF image of Cr_2O_3 $[2\bar{1}\bar{1}0]$ plane.

2.-Power, RF and energy storage applications

The forthcoming applications in the field of power and high-frequency electronics are going toward new designs for future devices as is the case for vertical transistors and implementation of two-dimensional (2D) materials, such as graphene (Gr), transition metal dichalcogenides (TMDs) and hexagonal boron nitride (h-BN).

To face the materials science issues related with the fabrication of these devices, atomic-column resolved analytical electron microscopy will address the origin of interface defects and probe the electronic properties at the atomic level to comprehensively understand the intrinsic mechanisms that rule the device operations.

Defects characterization of ion implanted P-doped 4H-SiC

Nowadays, 4H-SiC based devices are the key components in high-efficiency power conversion systems. Indeed, thanks to its excellent physical and chemical properties, Silicon Carbide appears as the best choice material able to push beyond the performance of Si-based power devices, which have reached by now the physical limits imposed by the material itself. Ion implantation is one of the most used methods for SiC doping in the microelectronic industry; nonetheless, the implanted ions are known to produce displacements along their path and a subsequent post-implant annealing is required to recover the crystalline phase and activate the dopants. However, extended defects, which are the by-product of implantation, constitute one of the main issues for high yield SiC-based devices. Typical ion implantation broad-band of defects induced by P implantation in SiC are reported in HAADF STEM image in Figure 12a.

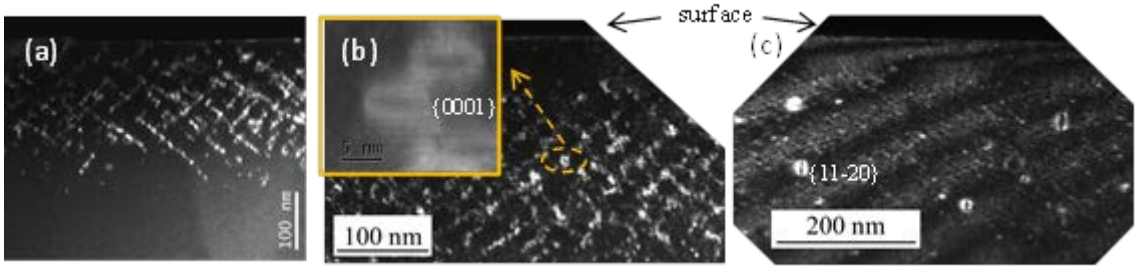

Figure 12. HAADF STEM image of the whole defect band (a), WBDF showing DLs with the habit plane parallel (b) and perpendicular (c) to the surface.

Moreover, in order to know the crystallographic characteristics of the defects conventional weak beam dark field (WBDF) demonstrate that these defects consist of dislocation loops (DLs) lying on the {0001} planes, parallel to the surface as shown in Figure 12b, and {11-20} planes, perpendicular to the surface (Figure 12c). While conventional WBDF allows the observation of the DL core and the evaluation of the Burger vector direction, Geometric Phase Analysis (GPA) technique, starting from High Resolution (HR) images, allows the evaluation of the Burger vector amplitude. CAT and CNRS-TOU are collaborating on the evaluation of the Burger vector corresponding to the different defects with the perspective of measuring the strain by electron holography. However, the first STEM and conventional HR images acquired in CAT don't allow a reliable interpretation of geometric phases because images are affected by fluctuations, probably due to charging effects occurring during STEM image acquisition. CAT is going

to test different acquisition conditions with the aim to prevent these problems and sending the new images to CNRS-TOU.

3.-Materials for advanced energy systems

Materials for advanced energy systems such as steam-generation, low footprint and "zero-emission" conventional power plants with increased efficiency need to incorporate new materials capable for operation at ultra-supercritical or advanced ultra-supercritical steam conditions in a temperature range up to 750°C for 100000 hours. Within this task, materials for advanced energy systems including fossil fuel power plants, clean coal technologies, nuclear power plants, renewables, smarts grids and energy storage will be investigated with new TEM techniques developed within WP4 and WP5.

Characterization of devices for Energy Applications: Heterostructure with Graphene layer deposited by CVD.

Well-established semiconductor materials, which build up the fundamental components of virtually any electronic device in use by modern society, have been subjected to a variety of nanostructures such as two-dimensional quantum wells, one-dimensional quantum wires/rods, and zero-dimensional quantum dots, these representing the most typical examples. Indium nitride provides an extra compelling example, and in our study kinetically stabilized 2D InN is explored in the context of the material concept for ultrathin "graphitic like" films of group III nitrides. The formation of this conceptual 2D material was harvested through targeted intercalation and deposition kinetics at the interface between hydrogen passivated SiC substrate and quasi-free-standing graphene using metal organic chemical vapour deposition (MOCVD) processes with precursors trimethylindium, $(CH_3)_3In$, and ammonia, NH_3. Within the framework of deposition kinetics controlled MOCVD processes we advance a material deposition platform for intercalated layers of In down to the limit of atomic thickness and diversity of chemical and structural arrangements. Intercalated layers of indium (InN) at the interface between hydrogen passivated SiC substrate and quasi-free-standing graphene giving origin to 2D InN_x were recorded by low e^- dose acquisition of annular bright-field (ABF) scanning transmission electron microscopy (STEM) images. In Figure 13, ABF- images of the intercalated layer are shown at atomic resolution. The SiC substrate appears at the bottom (zig-zag appearance) with two atomic layers of In, seen as dark dots. It is apparent that this layer is nucleated immediately on the SiC.

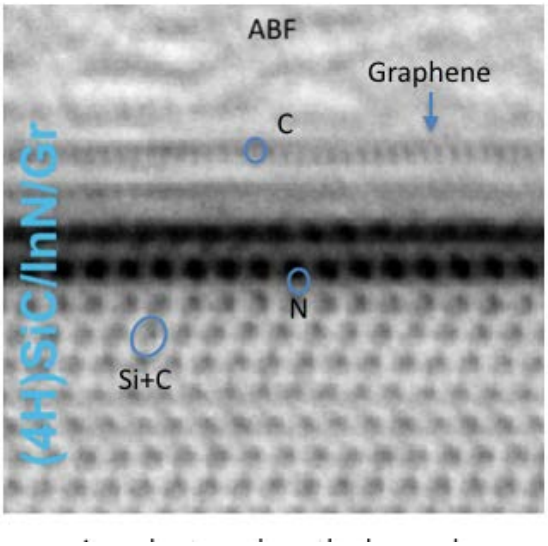

Figure 13. Low e^- dose ABF image of the intercalated InN layer aris shown at atomic resolution. The SiC substrate appears at the bottom (zig-zag appearance) with two atomic layers of In, seen as dark dots. It is apparent that this layer is nucleated immediately on the SiC. The image also clearly reports on the presence of grapheme on the top and N atoms bonded to the In atoms, SiC dimer is also revealed.

From the figure 13 is also possible to observe the presence of N atoms at the bottom of In atoms and regularly arranged C atoms of graphene above the intercalated InN bilayer. It apparent how STEM ABF in low dose acquisition configuration it is an impressive powerful approach which allow to harvest a whole class of information going from the direct atomic positions to the chemical information of both light (C, N) and heavy elements (SiC).

Task 8.4: Sample Preparation of Materials for Energy

Within this task, different methods for TEM sample preparation of materials/devices for energy applications will be optimised.

1.- New Sample Preparation Protocol for 2D materials

The preparation of a high quality specimen for TEM analysis is the first prerequisite to get great images and get rid to preparation artefacts. The mechanical exfoliation of Wan der Waals materials is one of the most promising ways to achieve good quality TEM lamella, but unfortunately they are mainly affected by the presence contaminant such as solvent or glue residual used for the exfoliation. The method we created is an improvement of the scotch tape method where we replaced the common sticky tape with a special ultraclean icros UV tape usually used as protective tape for silicon wafer back-grinding process in semiconductor manufacturing. In figure 14, we show the classical method, step by step, based on commercial low adhesive power scotch tape. Here multiple exfoliation steps are applied, each producing a slice with fewer layers, until only one remains. After exfoliation the flakes are deposited on a silicon wafer. Crystallites larger than 1 mm and visible to the naked eye [5]. Layers deposited on Si Wafer are transferred on a holey carbon TEM grid by a bed wetting of Ethanol.

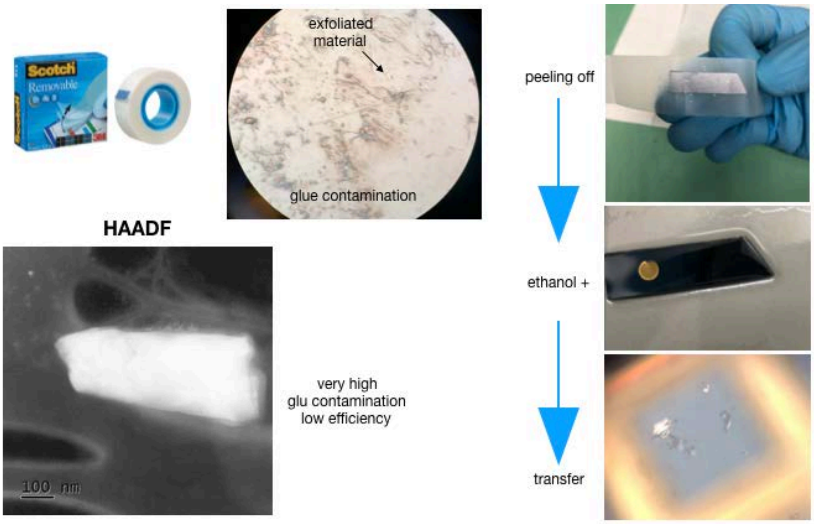

Figure 14. Classical mechanical exfoliation method for 2D materials showed step by step. Here commercial low adhesive power scotch tape has been used. After multiple exfoliation steps, each producing a slice with fewer layers, until only one remains. After exfoliation, the flakes are deposited on a silicon wafer. Layers are finally deposited on Si Wafer and transferred on a holey carbon TEM grid by a bed wetting of Ethanol. HAADF image shows a very glue contaminated specimen

Our new method is showed step by step in Figure 15. Here, after peeling the layers off many times, until only one remains, we deposited it on a silicon wafer than apply a UV flash to deactivate the glue. The surface of the wafer is now very clean end free of glue, thus implying a very clean transfer to the layer to the grid. A final wash of in Ethanol bath and KOH is applied in order to transfer the layer to the carbon holey carbon TEM grid.

In figure 16 (a-d) we show the cleanness of the wafer surface after the transfer of the layer on the wafer by using different sticky tape. Figure 12 (a) is the one obtained by using the ultraclean icros UV tape, from figures 16(b) to 16(c) other sticky tape were used as reported in the figure. It appears evident that the surface free of vax residual is the (a). The HAADF micrograph in figure 15 shows a very clean grid.

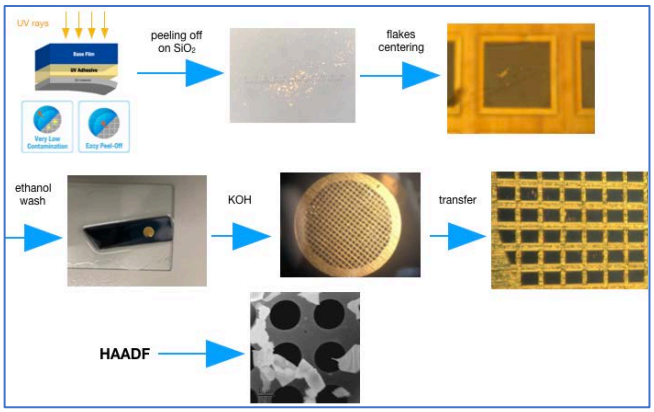

Figure 15. New exfoliation method based on ultraclean icros UV tape. After peeling the layer, we deposited it on a silicon wafer than apply a UV flash to deactivate the glue. The surface of the wafer is now very clean end free of glue, thus implying a very clean transfer to the layer to the grid. A final wash of in Ethanol bath and KOH is applied in order to transfer the layer to the carbon holey carbon TEM grid. HAADF image shows a very clean specimen.

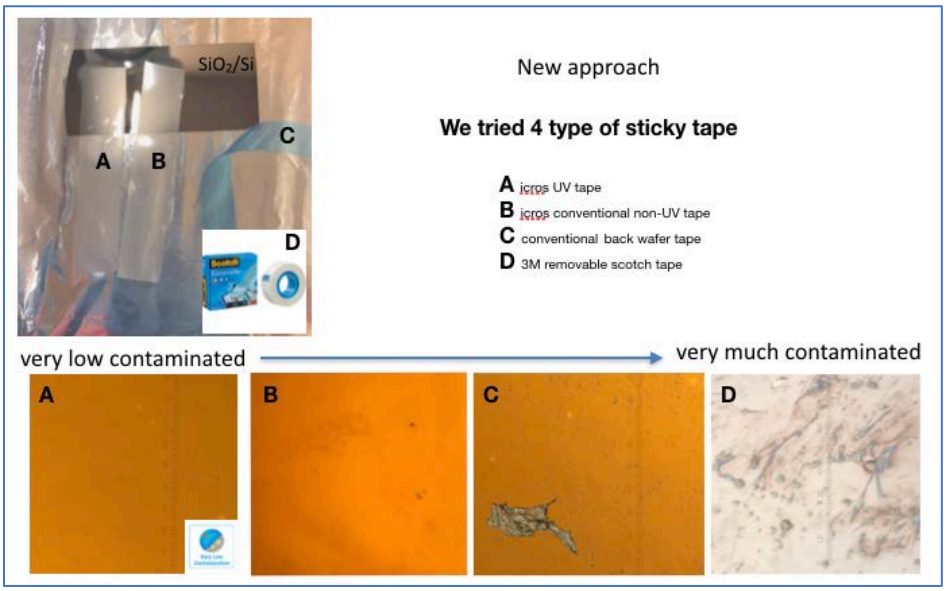

Figure 16. Comparison of Si wafer surface after layer transfer by different kind of sticky tape. From the comparison, it is apparent that the one transfered with the ultraclean icros UV tape is the cleanest

2.- Sample Preparation of ZnO monocrystals in desired orientation

For many studies it is necessary to prepare TEM sample of larger crystals (minerals) containing planar defects (e.g. IB) in desired crystal orientation. Very often one is encountered with the problem of a brittle nature of crystals when grinding and/or handling. One of the solutions is to glue a thin cylinder of the crystal in correct orientation (determined by XRD, EBSD) to a glassy support and then to thin it on both sides using tripod polishing approach in order to prepare thin parallel cuts prior to in-milling (Figure 17).

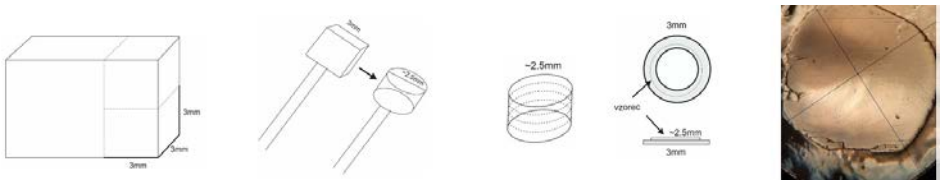

Figure 17. Work approach to prepare faulted crystals minerals in desired crystal orientation.

REFERENCES

1. Egelhaaf, H.J. and D. Oelkrug, *Luminescence and nonradiative deactivation of excited states involving oxygen defect centers in polycrystalline ZnO.* Journal of Crystal Growth, 1996. **161**(1-4): p. 190-194.
2. Suhadolnik, L., et al., *Influence of Anodization-Electrolyte Aging on the Photocatalytic Activity of TiO2 Nanotube Arrays.* Journal of Physical Chemistry C, 2020. **124**(7): p. 4073-4080.
3. Manzorro, R., et al., *Improving the Activity and Stability of YSZ-Supported Gold Powder Catalyst by Means of Ultrathin, Coherent, Ceria Overlayers. Atomic Scale Structural Insights.* Acs Catalysis, 2019. **9**(6): p. 5157-5170.
4. Lech, S., et al., *Three-dimensional imaging and characterization of the oxide scale formed on a polycrystalline nickel-based superalloy.* Scripta Materialia, 2019. **167**: p. 16-20.
5. Geim, A.K. and A.H. MacDonald, *Graphene: Exploring carbon flatland.* Physics Today, 2007. **60**(8): p. 35-41.